PHYSICAL REVIEW D **84,** 093001 (2011)

Higgs boson finder and mass estimator: The Higgs boson to WW to leptons decay channel at the LHC

Vernon Barger and Peisi Huang

Department of Physics, University of Wisconsin, Madison, Wisconsin 53706, USA

(Received 26 July 2011; revised manuscript received 29 September 2011; published 7 November 2011)

We exploit the spin and kinematic correlations in the decay of a scalar boson into a pair of real or virtual W-bosons, with both W-bosons decaying leptonically, for Higgs boson discovery at 7 TeV LHC energy with 10 fb^{-1} luminosity. Without reconstruction of the events, we obtain estimators of the Higgs mass from the peak and width of the signal distribution in m_{ll}. The separation of signal and background with other distributions, such as the azimuthal angle between two W decay planes, the rapidity difference between the two leptons, missing E_T, and the p_T of leptons, are also prescribed. Our approach identifies the salient Higgs to dilepton signatures that allow subtraction of the continuum $W*W*$ background.

DOI: 10.1103/PhysRevD.84.093001 PACS numbers: 14.80.Bn

The Higgs boson is the only missing brick of the standard model (SM) [1]. The $h \to W^+W^- \to l\nu l\nu$ channel has been of long interest for Higgs discovery [2–7] because of its relatively clean signal and the large branching fraction for m_h near $2m_W$. The CDF and D0 experiments at the Tevatron and the ATLAS and CMS experiments at the LHC have searched for the $h \to W^*W^* \to \mu\bar{\nu}_\mu\nu_\mu\bar{\mu}$ process and have excluded a SM Higgs in a range of m_h around 166 GeV [8–12]. The SM Higgs production cross section times the branching fraction to two W's in the SM is plotted in Fig. 1. The maximum $h \to W^*W^*$ signal from gluon fusion is at $m_h = 165$ GeV. The dominant production at $m_h < 1$ TeV occurs via the parton subprocess gluon + gluon $\to h$ and WW-fusion takes over at $m_h >$ 1 TeV [13]. Higgs production via gluon fusion could be larger than this estimate if extra colored states contribute to the gluon fusion loop [14], or it could be smaller if the weak coupling is shared by two neutral Higgs states, as would be the case in supersymmetry [15], or if the Higgs has invisible decay modes.

Many phenomenological studies have been made of the $h \to W^*W^*$ signal [16–20] and that of the closely related $h \to Z^*Z^*$ channel [21–25]. The $*WW*$ signal identification with leptonic $W*$ decay is challenging. With two missing neutrinos, the events are not fully reconstructible. Also, the $W*W*$ signal may have similar kinematics as the continuum $W*W*$ background. Since the background is much larger than the signal at the LHC, differences in the distributions of the signal and background must be used to identify and quantify the Higgs signal. A typical signal event in this channel for $m_h = 160$ GeV is shown in the N (number of events) vs η (rapidity difference of the leptons) vs ϕ (azimuthal angular difference of the leptons) plot in Fig. 2, along with that of a sample background event, illustrating that there can be distinguishing features. Our aim is to utilize the differences in the signal and background characteristics to enable a background subtraction and make a clear identification of any Higgs signal in novel ways that have not been fully explored in other studies. Our approach relies on the SM prediction of the background distributions from the $q\bar{q} \to W^*W^*$ subprocess at next-to-leading order (NLO) order [26] with the rejection of QCD jets. The theory normalization of this background can be tested in ranges of the distributions where the Higgs signal of a given m_H does not contribute. Also, diboson production with final states one W and one Z (WZ) production can serve as an independent calibration of the WW background, since the WZ final state does not have a neutral Higgs signal contribution. Our focus is on the dilepton signal with missing transverse energy and no jets. Other backgrounds, such as $t\bar{t}$ and single top production, can be suppressed by jet vetoing (for the zero jet signal), and the Drell-Yan background can be suppressed by a missing transverse energy requirement [27].

Nelson [28] investigated the correlation between the two W decay planes to distinguish the Higgs signal from the WW background. Choi *et al* [24,29] studied the signal distributions in transverse mass variables [30]. Dobrescu and Lykken [20] computed the fully differential width for Higgs decays to $l\nu jj$ and constructed distributions of $m_{l\nu}$, m_{jj}, polar (θ_l) and azimuthal (ϕ_l) angles between the charged lepton in the $l\nu$ rest frame and the W^+ in the Higgs rest frame, and θ_j, the angle between $-(\vec{p}_l + \vec{p}_\nu)$ and the fastest jet direction in the Higgs rest frame.

Estimating the Higgs mass from the invariant mass of two leptons,—The matrix element for the Higgs signal is similar to that of muon decay, except for the placement of muon spinor and inclusion of off shell W propagators [28]. We generated 200 000 events at four different Higgs mass points and $W*W*$ background with Sherpa [31], which includes the exact tree level matrix element and QCD radiation, at 7 TeV LHC center of mass (cm) energy. Jets are defined using the anti-kt algorithm [32] with $R = 0.4$, and the jet clusterings are implemented using the FASTJET package [33]. We use HIGGSDECAY [34] for calculation of the Higgs total and partial widths. We normalize the dilepton signal rate, $l = e,\ \mu$ for no jets to the

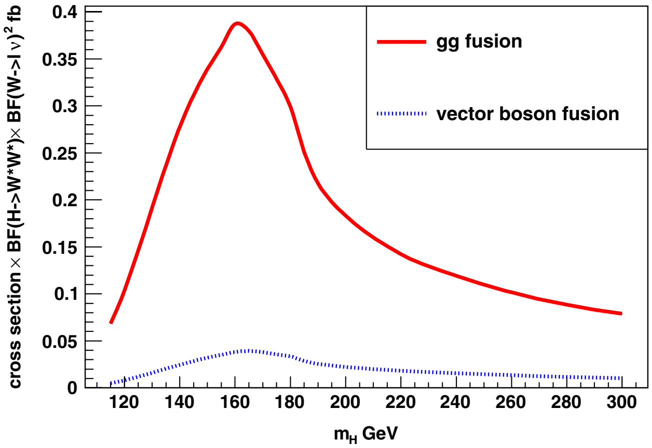

FIG. 1 (color online). SM Higgs production cross section times the branching fractions to two W's that decay leptonically. $l = e, \mu$.

next-to-next-to-leading order (NNLO) calculation [35], which is 104 fb at $m_H = 120$ GeV, 389 fb at $m_H = 160$ GeV, 182 fb at $m_H = 200$ GeV, and 83 fb at $m_H = 300$ GeV. The $WW \to l\nu l\nu$ background is normalized to the NLO prediction [36] of 2095 fb. These cross sections are for the dilepton final states with $l = e, \mu$ including the leptonic branching fractions. The m_{ll} distributions, with and without the WW background, are given in Fig. 3, each for 1 fb^{-1} integrated luminosity. The width (w) of the m_{ll} distribution is given in Fig. 4. This width is large compared

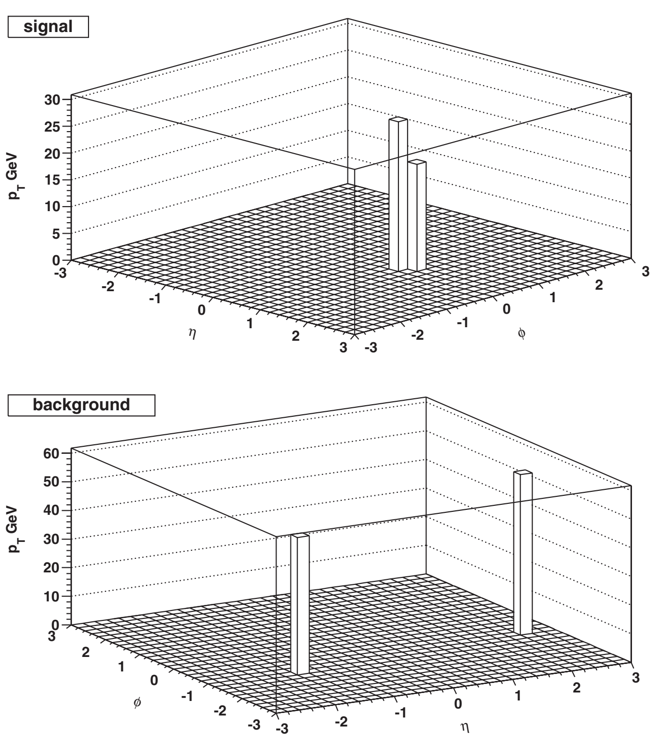

FIG. 2. Sample events for the $m_h = 160$ GeV signal and the $W*W*$ background with no jets.

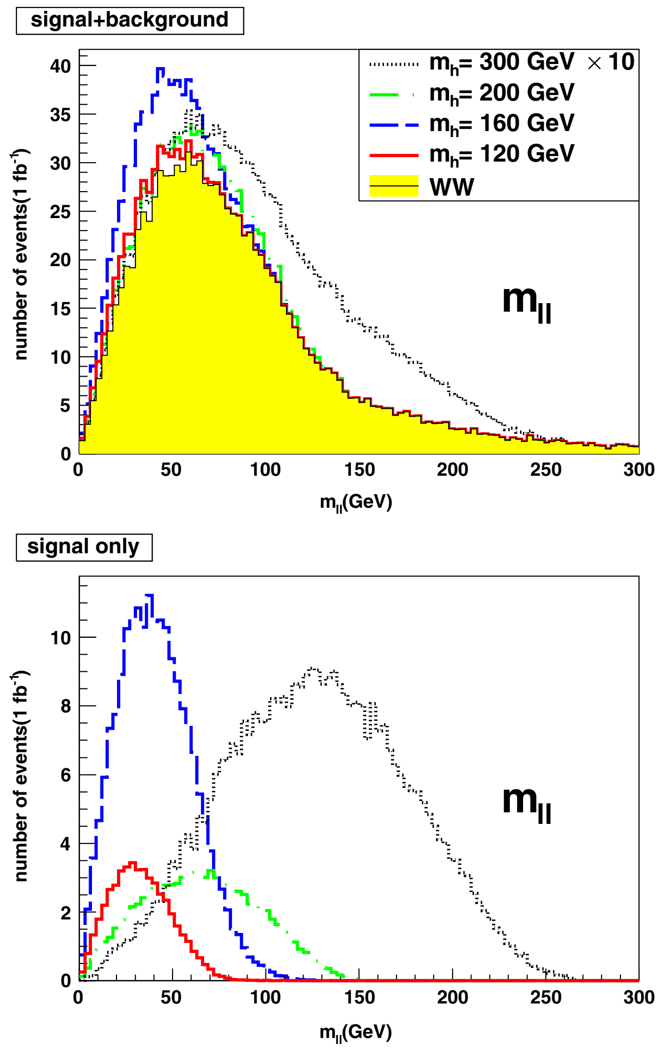

FIG. 3 (color online). m_{ll} event distribution of the SM Higgs signal at various m_h and the background from continuum $W*W*$ production for 1 fb^{-1} luminosity at 7 TeV, summed over $l = e, \mu$

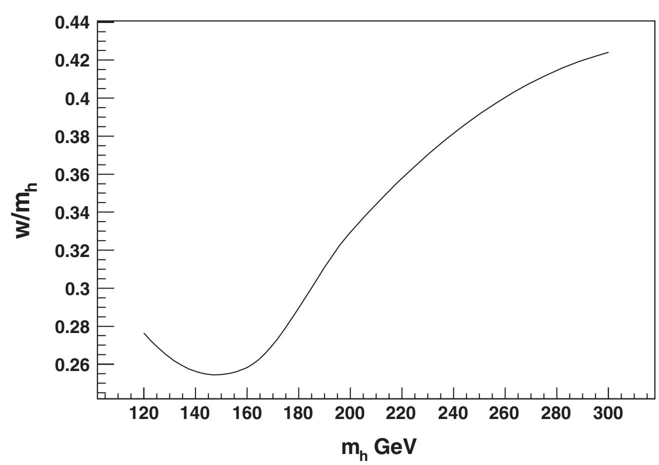

FIG. 4. Width (w) of the m_{ll} distribution of the Higgs signal compared to m_h. Note that at $m_h = 150$ GeV(200 GeV), w $= \frac{1}{4} m_h$(w $= \frac{1}{3} m_h$).

TABLE I. The signal and WW continuum background events at 7 TeV within the specified m_{ll} windows around the peak values. The number of events in the signal and background columns are for 10 fb^{-1} integrated luminosity anticipated from ATLAS and CMS combined. Event numbers are summed over $l = e, \mu$. No experimental cuts are applied here

m_h (GeV)	m_{ll} window (GeV)	Signal inside window	Background inside window	Background outside window
120	10–50	373	2746	7723
160	20–70	1478	4326	6144
200	30–110	687	6713	3756
300	60–200	324	5901	4568

to the total decay width of the Higgs boson, making it sensitive only to the Higgs mass. Here we only require two leptons and no jets, with no acceptance cuts.

The following empirical relationship between m_H and m_{ll} of the signal is found, where "peak" is the maximum and "end" is the end point of the m_{ll} distribution.

$$m_H = 2(m_{ll\mathrm{peak}}) + m_W \qquad m_H = m_{ll\mathrm{end}} + \frac{m_W}{2}. \tag{1}$$

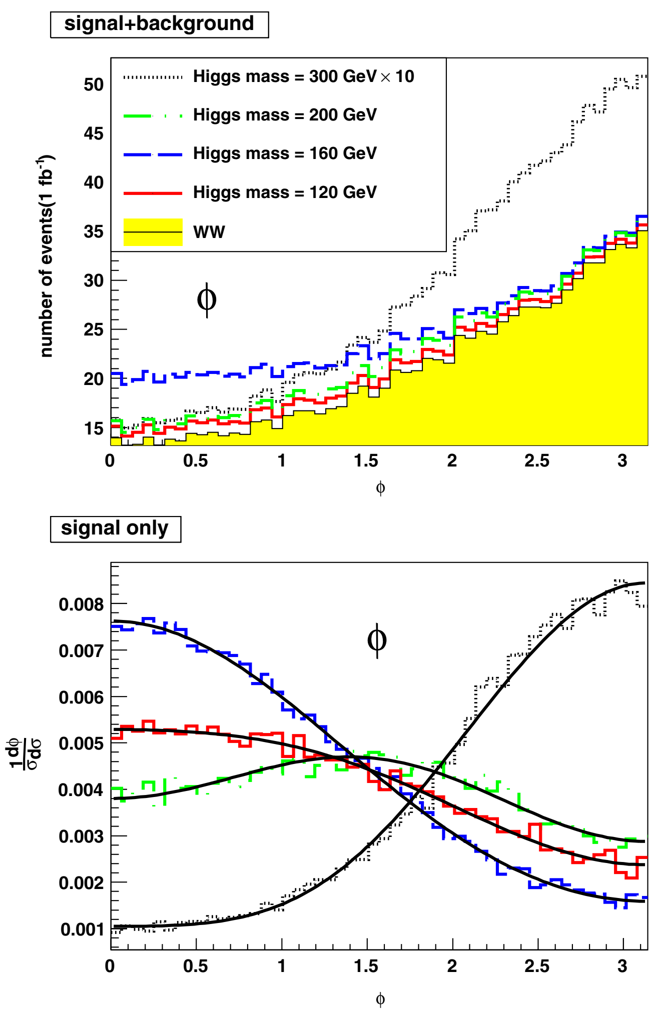

FIG. 5 (color online). The azimuthal angle between the two W decay planes, before cuts.

This relationship holds for all the Higgs mass points, including when one W is off shell, near the $2m_W$ threshold and well above the threshold. The signal and $W*W*$ background within windows around the peak values of m_{ll} are listed in Table I. In addition, we find a rather tight correlation of the Higgs mass with the width of the m_{ll} distribution, as discussed below.

Parametrization of the azimuthal angular distribution.— The correlation function for the azimuthal angle between the two W decay planes can be parametrized as [28]

$$F(\phi) = 1 + \alpha \cos\phi + \beta \cos 2\phi. \tag{2}$$

The direction of the normal to a W decay plane is defined as the cross product of momentum direction of the lepton with the beam direction. In Fig. 5 we plot the ϕ distribution of signal and the WW background and fit the normalized distributions to Eq. (2). The resulting α and β values are given in Table II.

It can be seen that $\alpha > 0$ in the transverse-transverse (TT) dominant region, while $\alpha < 0$ in the longitudinal-longitudinal (LL) dominant region. At $m_H = 1 + \sqrt{17} m_W = 182$ GeV, $\Gamma(h \to W_T W_T) = \Gamma(h \to W_L W_L)$. The ϕ distribution at $m_H = 200$ GeV is almost flat, as expected. The WW background has $\alpha < 0$ because it is LL dominant. The ϕ distributions within different m_{ll} bins are shown in Fig. 6. In the $m_{ll} < 50$ GeV bin, signal and background are both dominantly TT, and in the high m_{ll} bin, both are dominantly LL.

The pseudorapidity difference $\Delta\eta = |\eta_1 - \eta_2|$ of the two leptons is plotted in Fig. 7. Note that the charged leptons from signal are closer in $\Delta\eta$ than for the background.

Background estimation.— Other variables can also differentiate signal from the background, such as $\not{E}_T = p_T(ll)$

TABLE II. The α and β parametrization from fit of Eq. (2) to the ϕ distributions

Higgs mass (GeV)	120	160	200	300	Background
α	0.36	0.68	0.12	−0.95	−0.43
β	−0.06	0.04	−0.17	0.22	0.09

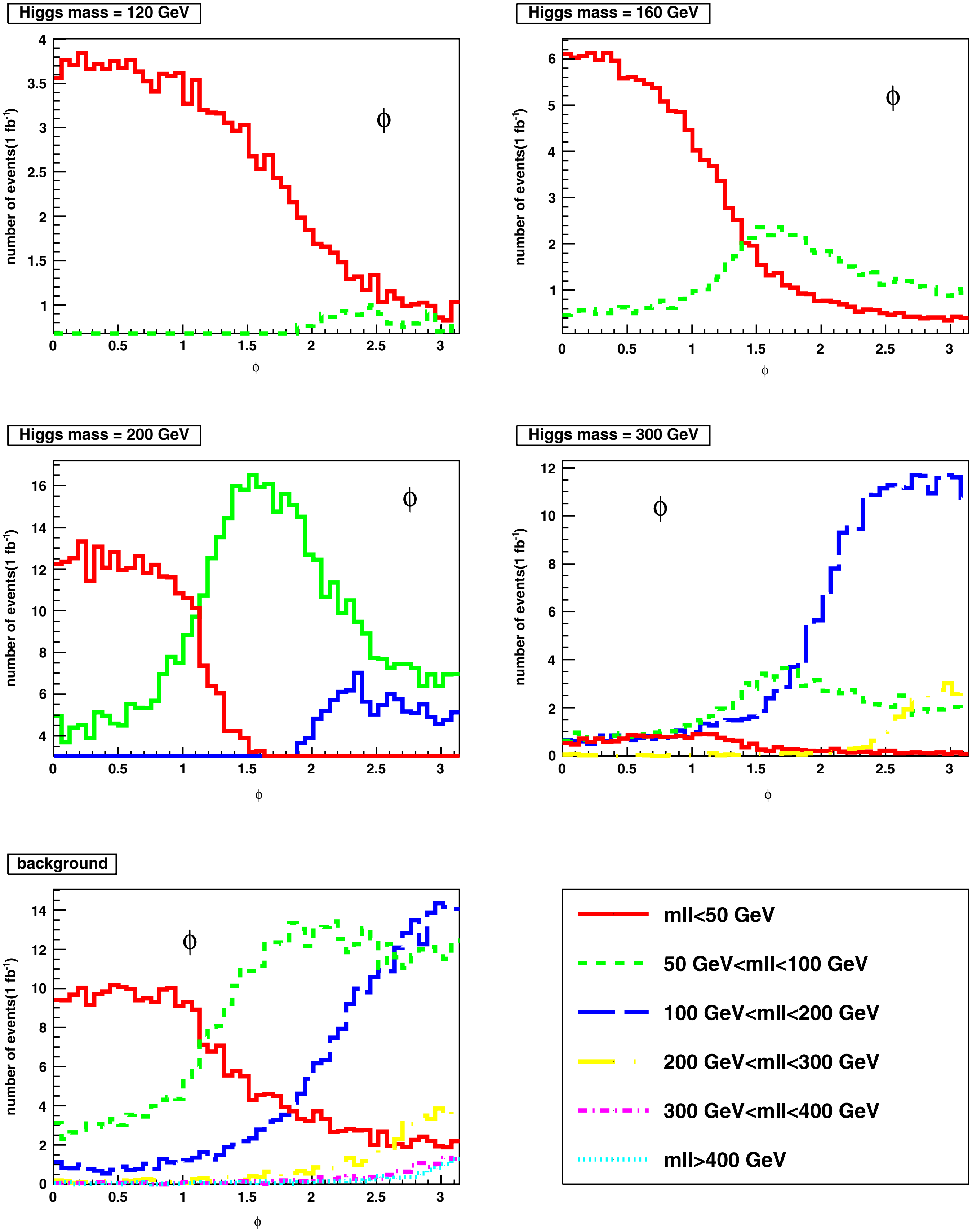

FIG. 6 (color online). ϕ distributions in different m_{ll} bins of the Higgs signals and the background, before cuts.

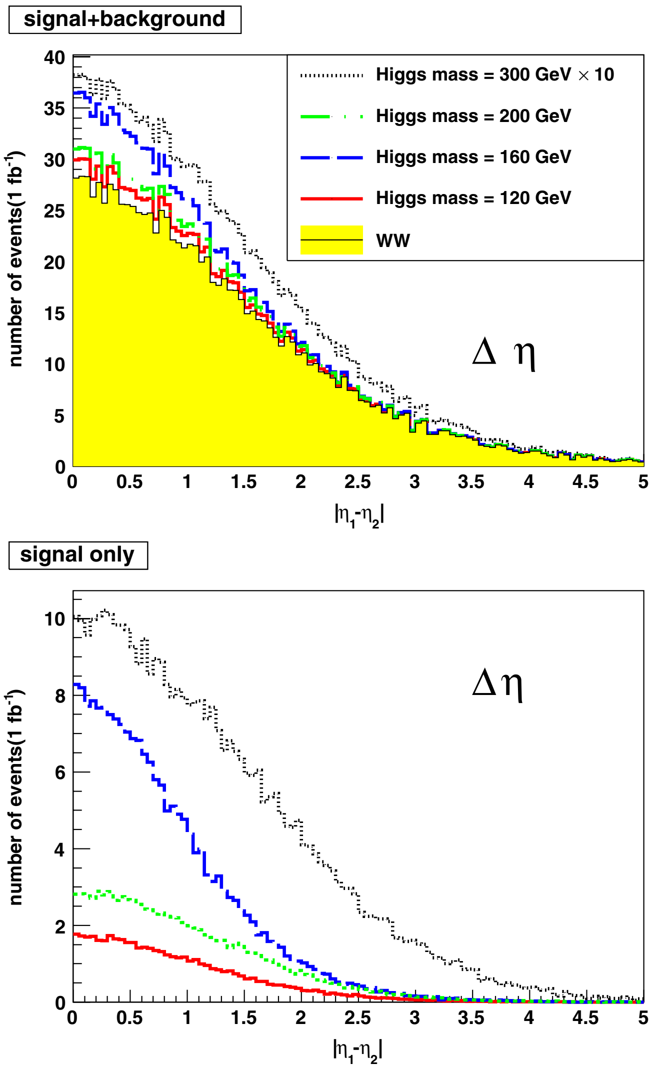

FIG. 7 (color online). Pseudorapidity difference $\Delta\eta =| \eta_1 - \eta_2 |$ of the two leptons, before cuts.

and the p_T distribution of the fastest lepton, p_{T1}, shown in Fig. 8.

The p_T distribution of the fastest lepton is very sensitive to the Higgs mass. This distribution is sharply peaked for $m_h = 160$ GeV. A recent proposed variable, ϕ^* [37], is plotted in Fig. 9. ϕ^* is defined as $\phi^* = \tan[(\pi - \phi)/2] \times \sin\theta^*$, where ϕ is the azimuthal angle between the two leptons and $\cos\theta^* = \tanh[(\eta^- - \eta^+)/2]$, with η^- (η^+) being the pseudorapidity of the negatively charged lepton. It has been argued that ϕ^* may be more precisely determined than ϕ.

The sum of the energy of the two leptons is shown in Fig. 10. The peak value of the $E(l^+) + E(l^-)$ distribution of the signal is corelated with m_H.

Application of acceptance cuts for background rejection.— Other backgrounds include $t\bar{t}$ pair production, single top production, W(or Z) + jets, the Drell-Yan process (which does not contribute to the $e\mu$ events), and $\tau\bar{\tau}$

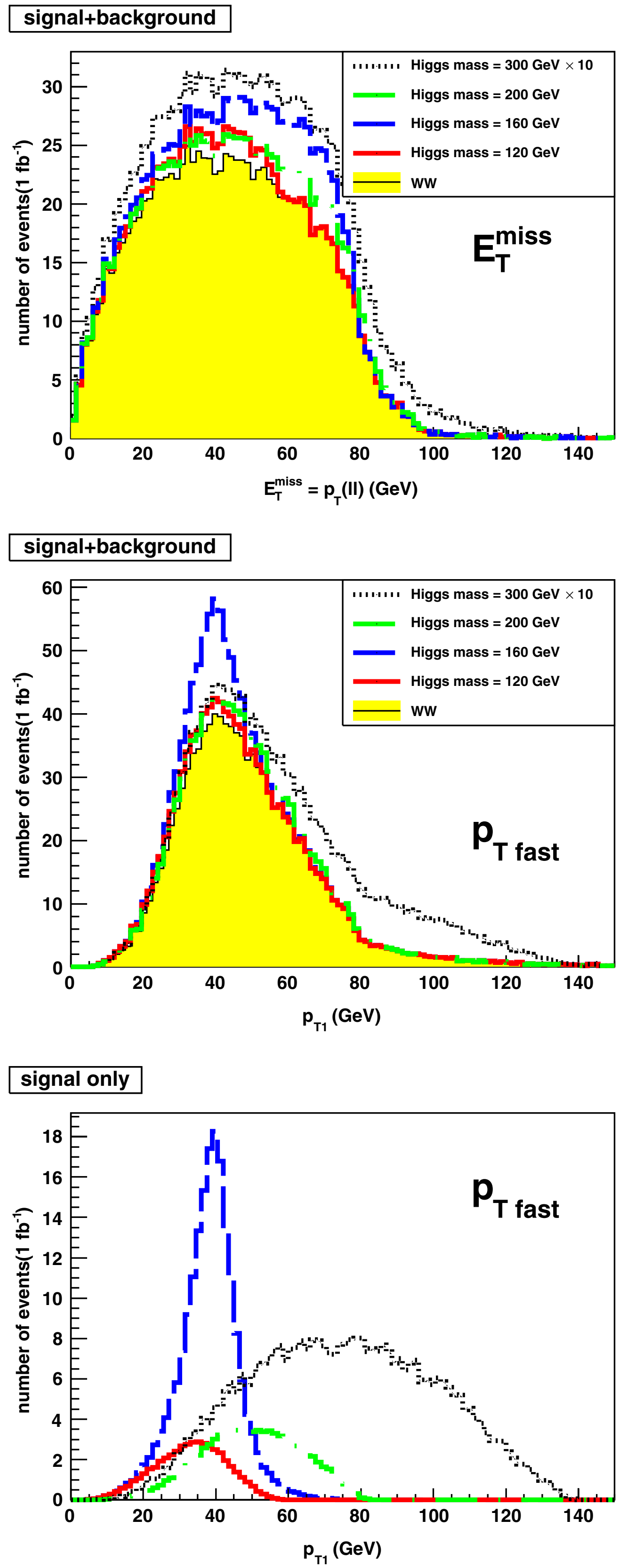

FIG. 8 (color online). The $\not{E}_T = pT(ll)$ distribution and the p_T distribution of the fastest lepton, before cuts. Note the sharply peaked p_{T1} from $m_H = 160$ GeV.

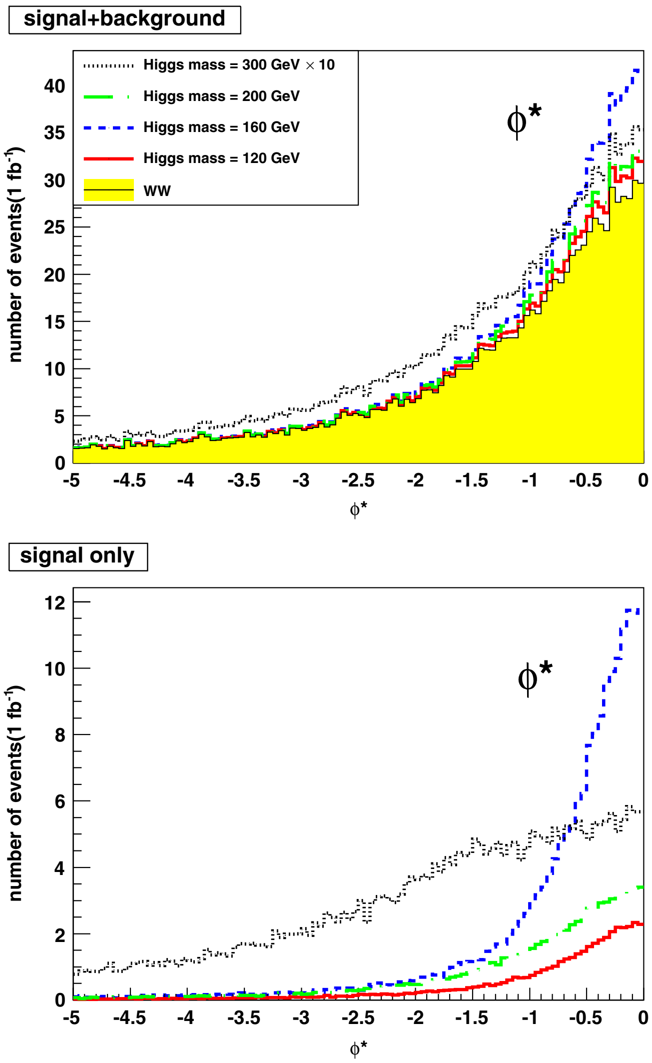

FIG. 9 (color online). ϕ^* distribution, before cuts.

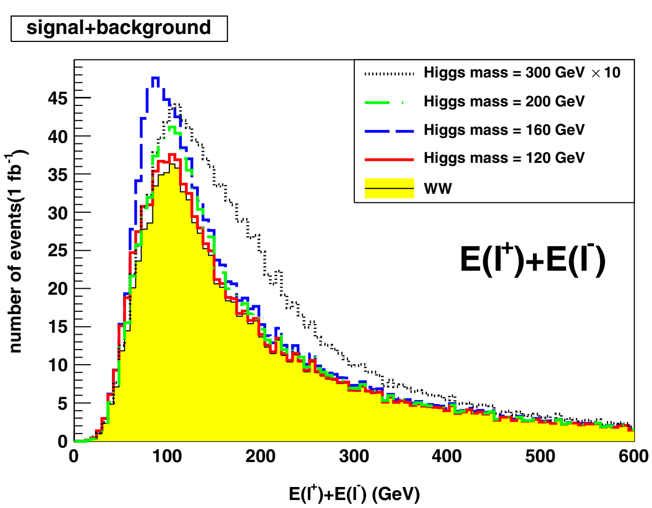

FIG. 10 (color online). Sum of energy of the two leptons, before cuts.

production. All these backgrounds can be suppressed by vetoing the jets and suitable cuts on the distributions of the variables discussed above. We apply cuts following a recent ATLAS study [27].

(i) Cut 1: no jets.
(ii) Cut 2: $m_{ll} > 15$ GeV.
(iii) Cut 3 :$E_T > 30$ GeV.
(iv) Cut 4: $p_T^{ll} > 30$ GeV.
(v) Cut 5: $\delta\phi_{ll} < 1.8$.

Figure 11 shows that the shape of the m_{ll} distribution does not change under those cuts.

The ϕ distribution after experimental cuts is shown in Fig. 12. The TT component is reduced by the m_{ll} cut.

The analysis of ATLAS shows that all the backgrounds except $W*W*$ can be suppressed by cuts similar to those

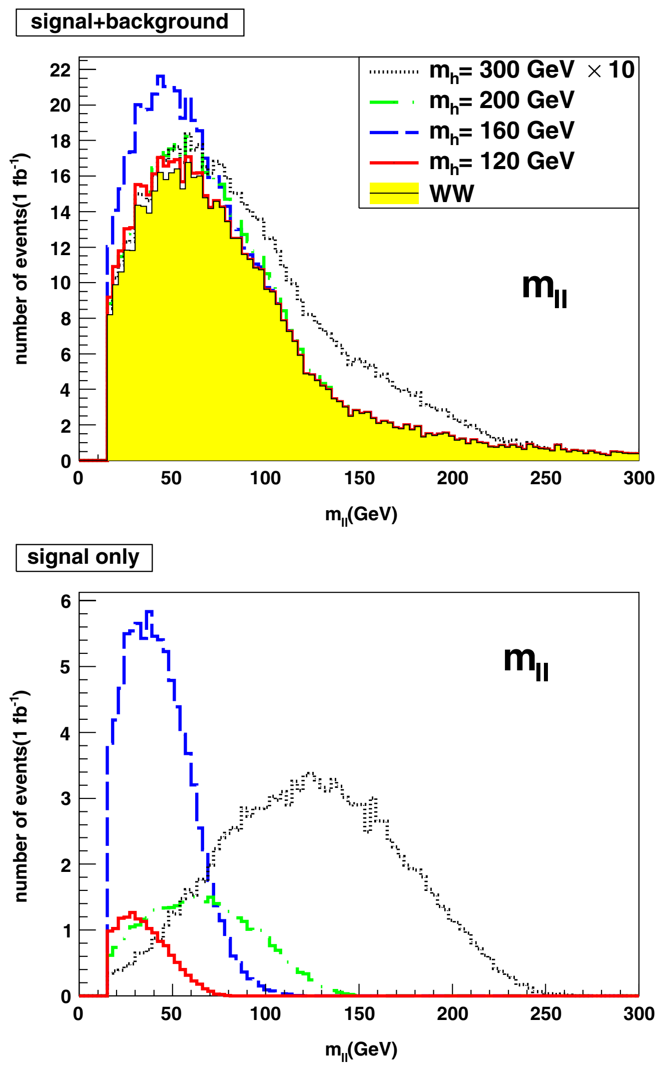

FIG. 11 (color online). m_{ll} event distribution, after cuts, of the SM Higgs signal (for various m_h) and the continuum $W*W*$ background for 1 fb^{-1} luminosity at 7 TeV, summed over $l = e, \mu$

TABLE III. The signal and background events at 7 TeV, after cuts, within the specified m_{ll} windows around the peak values. The number of events in the signal and background columns are for 10 fb^{-1} integrated luminosity anticipated from ATLAS and CMS combined. Event numbers are summed over $l = e, \mu$.

m_h (GeV)	m_{ll} window (GeV)	Signal inside window	WW inside window	$t\bar{t}$ inside window	Background inside window	WW outside window	$t\bar{t}$ outside window	Background outside window
120	15–50	45	638	151	789	743	118	861
160	20–70	303	899	189	1088	482	80	562
200	30–110	88	1022	220	1242	359	49	408
300	60–200	16	530	89	619	851	180	1031

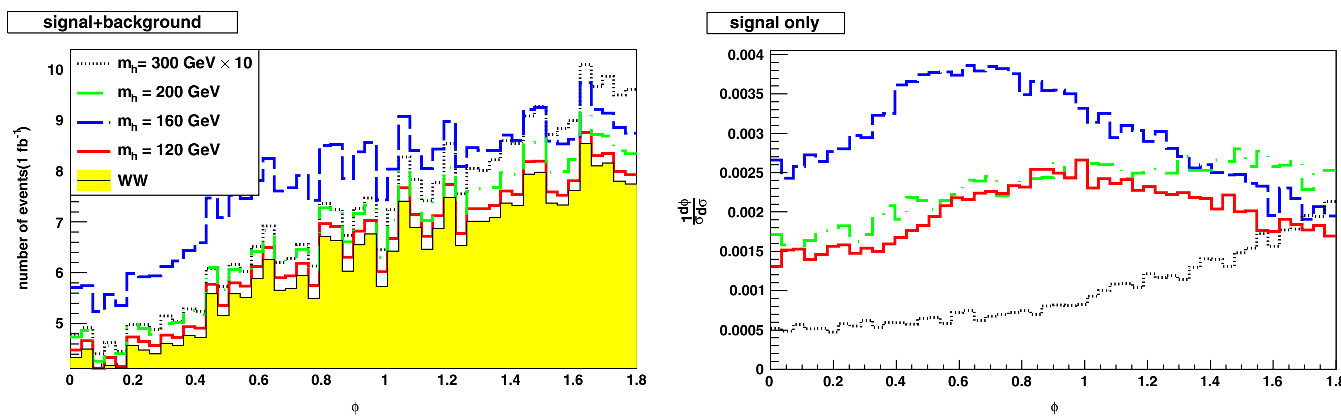

FIG. 12 (color online). The azimuthal angle between the two W decay planes, after cuts.

given above [27]. Table III shows signal and backgrounds within windows around peak value of m_{ll} after application of those cuts. Multivariable techniques, such as neural networks and boost decision trees, are another effective approach to background rejection.

Conclusions and outlook.—After subtracting the WW continuum background from the dilepton data, the Higgs mass can be estimated using Eq. (1). The width of the m_{ll} distribution provides another good estimator of the Higgs mass. The m_{ll}, p_T, and E distributions are truncated at their lower ends by the p_T and η acceptance cuts.

Our analysis techniques can be applied to scalars in other models that decay via the WW mode such as the radion [38–43] or a dilaton [44]. The merit of the m_{ll} peak estimator in Eq. (1) and width estimator in Fig. 4 is their simple dependences on the Higgs boson mass.

This work was supported in part by the U.S. Department of Energy under Grant No. DE-FG02-95ER40896.

[1] Abdelhak Djouadi, Phys. Rep. **457**, 1 (2008).
[2] Wai-Yee Keung and W. J. Marciano, Phys. Rev. D **30**248 (1984).
[3] E. W. N. Glover, J. Ohnemus, and Scott S. D. Willenbrock, Phys. Rev. D **37**, 3193 (1988).
[4] V. Barger, G. Bhattacharya, T. Han, and B. A. Kniehl, Phys. Rev. D **43**, 779 (1991).
[5] V. Barger, Kingman Cheung, T. Han, and D. Zeppenfeld, Phys. Rev. D **44**, 2701 (1991).
[6] Vernon D. Barger, Kingman Cheung, Tao Han, and D. Zeppenfeld, Phys. Rev. D **48**, 5433 (1993).
[7] Tao Han, André S. Turcot, and Ren-Jie Zhang, Phys. Rev. D **59**, 093001 (1999).
[8] T. Aaltonen *et al.*, Phys. Rev. Lett. **104**, 061802 (2010).
[9] T. Aaltonen *et al.*, Phys. Rev. Lett. **104**, 061803 (2010).
[10] Victor Mukhamedovich Abazov *et al.*, Phys. Rev. Lett. **106**, 171802 (2011).
[11] Georges Aad *et al.*, Limits on the Production of the Standard Model Higgs Boson in pp Collisions at sqrt(s) = 7 TeV With the ATLAS Detector (2011).
[12] Serguei Chatrchyan *et al.*, Phys. Lett. B **699**, 25 (2011).
[13] S. Dittmaier *et al.*, Handbook of LHC Higgs Cross Sections: 1. Inclusive Observables (2011).
[14] Qiang Li, Michael Spira, Jun Gao, and Chong Sheng Li, Phys. Rev. D **83**, 094018 (2011).
[15] Robert Harlander, Eur. Phys. J. C **33**, s454 (2003).
[16] Tao Han and Ren-Jie Zhang, Phys. Rev. Lett. **82**, 25 (1999).

[17] Edmond L. Berger, Qing-Hong Cao, C. B. Jackson, Tao Liu, and Gabe Shaughnessy, Phys. Rev. D **82**, 053003 (2010).
[18] Charalampos Anastasiou, Guenther Dissertori, Massimiliano Grazzini, Fabian Stockli, and Bryan R. Webber, J. High Energy Phys. 08 (2009) 099.
[19] Alan J. Barr, Ben Gripaios, and Christopher Gorham Lester, J. High Energy Phys. 07 (2009) 072.
[20] Bogdan A. Dobrescu and Joseph D. Lykken, J. High Energy Phys. 04 (2010) 083.
[21] M. J. Duncan, Phys. Lett. B **179**, 393 (1986).
[22] C. Zecher, T. Matsuura, and J. J. van der Bij, Z. Phys. C **64**, 219 (1994).
[23] C. P. Buszello, I. Fleck, P. Marquard, and J. J. van der Bij, Eur. Phys. J. C **32**, 209 (2004).
[24] Kiwoon Choi, Suyong Choi, Jae Sik Lee, and Chan Beom Park, Phys. Rev. D **80**, 073010 (2009).
[25] Yanyan Gao, Andrei V. Gritsan, Zijin Guo, Kirill Melnikov, Markus Schulze, and Nhan V. Tran, Phys. Rev. D **81**, 075022 (2010).
[26] J. Ohnemus, Phys. Rev. D **50**, 1931 (1994).
[27] ATLAS Collaboration, Report No. ATLAS-CONF-2011-005, Geneva, 2011.
[28] Charles A. Nelson, Phys. Rev. D **37**, 1220 (1988).
[29] Kiwoon Choi, Jae Sik Lee, and Chan Beom Park, Phys. Rev. D **82**, 113017 (2010).
[30] V. Barger and R. J. Phillips, *Collider Physics* (Addison-Wesley, Reading, MA, 1987).
[31] T. Gleisberg *et al.*, J. High Energy Phys. 02 (2009) 007.
[32] Matteo Cacciari, Gavin P. Salam, and Gregory Soyez, J. High Energy Phys. 04 (2008) 063.
[33] Matteo Cacciari and Gavin P. Salam, Phys. Lett. B **641**, 57 (2006).
[34] A. Djouadi, J. Kalinowski, and M. Spira, Comput. Phys. Commun. **108**, 56 (1998).
[35] Julien Baglio and Abdelhak Djouadi, J. High Energy Phys. 03 (2011) 055.
[36] H Yang, Report No. ATL-COM-PHYS-2010-1012, 2011.
[37] A. Banfi, S. Redford, M. Vesterinen, P. Waller, and T. R. Wyatt, Eur. Phys. J. C **71**, 1600 (2011).
[38] Walter D. Goldberger and Mark B. Wise, Phys. Lett. B **475**, 275 (2000).
[39] Kingman Cheung, Phys. Rev. D **63**, 056007 (2001).
[40] Thomas G. Rizzo, J. High Energy Phys. 06 (2002) 056.
[41] Graham D. Kribs, arXiv:hep-ph/0605325.
[42] Hooman Davoudiasl, Thomas McElmurry, and Amarjit Soni, Phys. Rev. D **82**, 115028 (2010).
[43] Yochay Eshel, Seung J. Lee, Gilad Perez, and Yotam Soreq, arXiv:1106.6218.
[44] Walter D. Goldberger, Benjamín Grinstein, and Witold Skiba, Phys. Rev. Lett. **100**, 111802 (2008).